

ANDRZEJ KWINTA¹*, ANNA KOPEĆ²**MODELLING THE GEOMETRY OF DISPLACEMENTS CAUSED BY MINING-INDUCED TREMORS BASED ON InSAR MEASUREMENTS**

Mining-induced seismic events generate ground surface displacements that can significantly impact infrastructure. This study presents a geometric analysis of ground surface displacements caused by mining-induced tremors using remote sensing techniques, particularly Differential Interferometric Synthetic Aperture Radar (DInSAR). The research focuses on two seismic events in the Legnica-Głogów Copper District (LGCD), Poland, examining displacement fields through SAR imagery from Sentinel-1 satellites. The Geometry of the displacement field was described with a function of stochastic medium displacement and Aviershin's observation. The centre of gravity of the displacement field, its impact radius, and proportionality coefficient for vertical and horizontal displacement were determined. The results confirm the suitability of this model in describing mining-induced subsidence troughs, with high agreement between measured and calculated displacement values. Additionally, the study identifies systematic deviations in DInSAR - derived measurements, suggesting necessary corrections for improved accuracy. The findings contribute to a better understanding of ground surface deformation process and offer insights into refining predictive models for mining-induced subsidence.

Keywords: Surface deformation; InSAR data; mining-induced tremor; displacement model; fit of theoretical model to displacement field

1. Introduction

Mining is detrimental to all components of the natural environment [1,2]. Nevertheless, dynamic technology change requires mineral extraction. The general public perceives fossil fuels as the most dangerous for the environment and climate change. Displacement of large areas of the surface is not necessarily linked to the extraction of fossil fuels. It can be caused by groundwater withdrawal for agriculture or cities [3-7] or earth seismicity [8].

¹ LAND SURVEYING, UNIVERSITY OF AGRICULTURE IN KRAKOW, BALICKA 253A, 30-149, KRAKOW, POLAND

² WROCLAW UNIVERSITY OF SCIENCE AND TECHNOLOGY, FACULTY OF GEOENGINEERING, MINING AND GEOLOGY, NA GROBLI 15, 50-421 WROCLAW, POLAND

* Corresponding author: andrzej.kwinta@urk.edu.pl



© 2025. The Author(s). This is an open-access article distributed under the terms of the Creative Commons Attribution License (CC-BY 4.0). The Journal license is: <https://creativecommons.org/licenses/by/4.0/deed.en>. This license allows others to distribute, remix, modify, and build upon the author's work, even commercially, as long as the original work is attributed to the author.

The effects of underground mining recorded on the surface can have diverse causes. Researchers have long attempted to propose an adequate classification of the impacts [1,9,10]. One of them is categorising direct, indirect, and secondary impacts, although direct-indirect division might seem more reasonable. Direct impacts are any deformation movements related to a void in the rock mass and its upward migration. Indirect impacts would cover all additional deformation phenomena observed on the surface related to mining but not caused directly by mineral extraction. Some are paraseismic tremors [11-15], rock mass drains from aquifer damage, or mine flooding [16]. While the modelling of direct deformations has been relatively well described [1,9], the modelling of indirect deformation is often difficult to describe. Direct mining-related deformations can be modelled satisfactorily [17], making it possible to predict extreme values of indicators, where they will occur, whether they will occur, and what the impact range will be [18,19]. In the case of indirect deformation, when predictive capabilities are limited, one can focus solely on describing the effects with measured values.

Mining tremors are the rapid discharge of stresses caused by mining operations, manifested by the dynamic movement of the rocks forming the rock mass, with Crump being a similar phenomenon. In addition, there is a loss of stability in the excavation, and the rock material is cast into it. In the case of a tremor, the subsidence trough that is related to the void caused by mining operations and accumulated in the rock mass. The tremor, through the movement of the rock mass, accelerates the exposure of this previously accumulated void on the ground surface. Deformations associated with mining tremors are localised in already existing areas of subsidence [12,13]. Thus, indirect influences resulting from induced seismic tremors intensify direct influences. The classical measurement methods for monitoring mining-induced deformations are general land surveying methods (vertical and horizontal measurements) [20]. Thanks to advances in surveying technology, deformations can be measured with GNSS [21-24] or integrated networks (combined classical and GNSS measurements) [25]. The next step on the developmental path of measurements in mining areas was satellite remote sensing, especially radar interferometry [26-28]. In the case of classical surveying methods, observations are spatially and temporarily discrete, and any disturbances result in deformation analysis issues. When surveying networks are elongated enough, indirect impacts due to rock mass drain can be measured. Still, the necessity to tie in to 'fixed points' (outside the deformation) [18] over large distances is cost- and time-intensive. Classical measurements of deformations from tremors are problematic. It is difficult to plan the 'zero' measurement as the time and place of tremors are unpredictable. The advent of GNSS streamlined the measurement of deformations in mining areas. The measurement can be performed continuously with the use of permanent stations [24]. Regrettably, these are merely individual points in space. Satellite remote sensing addresses the spatial issue of imaging because a single image can encompass an entire mining district. The only problem can be the revisit time, which affects the imaging interval. After Interferometric Synthetic Aperture Radar (InSAR) was introduced, first attempts were made to apply it to deformation monitoring [26,29]. The technology was initially expensive (high costs of imagery), and revisit times were relatively long (35 days for ENVISAT). Today, these two fundamental issues grow irrelevant thanks to the abundance of satellites and free access to Sentinel-1 imagery under the European Space Agency (ESA) programme Copernicus Sentinel. InSAR measurements yield information on both direct and indirect deformations. Researchers can integrate satellite imagery with classical surveying [30].

The paper presents a geometric analysis of remote sensing imaging of a surface undergoing deformation due to mining-induced tremors [14,31]. Frequent satellite revisits and diverse orbits (ascending and descending) provide completely new information about the course of

mining-induced deformation. It is an attempt to describe the geometry of a surface undergoing deformation as a result of a mining-induced tremor. The conclusions will help to understand the rock mass and surface deformation process caused by mining-induced tremors.

2. Determination of displacements with SAR imagery

SAR imagery is dynamically gaining popularity in deformation monitoring caused by underground technology, especially the influence of mining exploitation. Preliminary research from the late twentieth century has moved to an intensive phase and is broadly applied [32,33]. Hardly a month goes by without a new research paper on the topic. The availability of images shared by ESA under the Copernicus Sentinel programme drives multifaceted analyses of deformation. The present paper used data from Sentinel 1 A/B satellites that acquire large quantities of data from extensive areas that include the effects of mining activity.

Surface deformations were measured using the Differential Interferometric Synthetic Aperture Radar (DInSAR) method. The broad procedure for determining displacement with SAR data is shown in Fig. 1 [34]. It is rather general and presents key stages of transition from two radar images to georeferenced displacements.

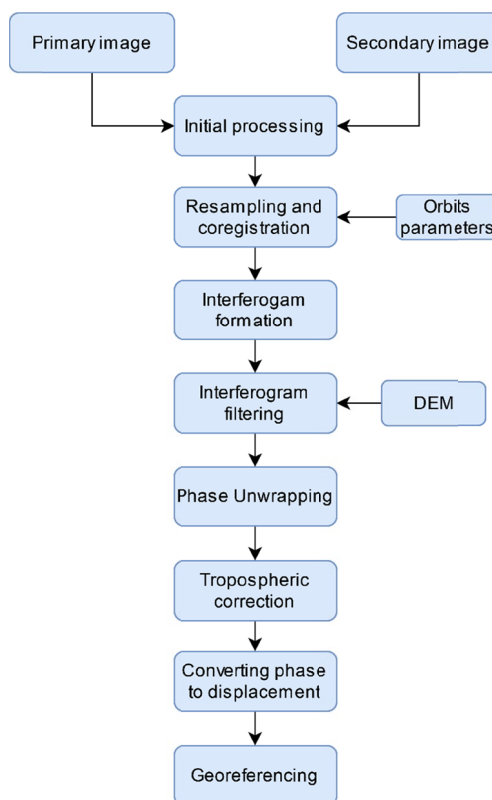


Fig. 1. Identification of displacements in SAR images [34]

Computations were performed in GMTSAR [35]. Each stage of the computations required an adequate processing model and a matching set of parameters. Incorrect parameters may distort results. Thanks to the expertise and classical measurements, knowledge of the course of the process facilitates proper verification of the computational models and their parameters [34]. Interferogram phase unwrapping was conducted with a Statistical-cost Network-flow Algorithm for Phase Unwrapping (SNAPHU) [36]. The employed statistical model accounted for potential land surface deformations [37]. The tropospheric effect was reduced with the Generic Atmospheric Correction Online Service for InSAR (GACOS) based on the Iterative Decomposition Model (ITD) [38].

Based on observations from a single path, it is possible to determine displacements in only one direction – along the line of sight (LOS). At least three satellites moving in different directions would be needed to obtain a spatial insight into the displacements (in the vertical and horizontal planes) (1):

$$\begin{bmatrix} U_{LOS1} \\ U_{LOS2} \\ \dots \\ U_{LOSn} \end{bmatrix} = \begin{bmatrix} -\sin \theta_1 \cos \alpha_1 & \sin \theta_1 \sin \alpha_1 & \cos \theta_1 \\ -\sin \theta_2 \cos \alpha_2 & \sin \theta_2 \sin \alpha_2 & \cos \theta_2 \\ \dots & \dots & \dots \\ -\sin \theta_n \cos \alpha_n & \sin \theta_n \sin \alpha_n & \cos \theta_n \end{bmatrix} \begin{bmatrix} U_{WE} \\ U_{SN} \\ U_H \end{bmatrix} \quad (1)$$

where:

- $U_{LOS1}, U_{LOS2}, \dots, U_{LOSn}$ – slant displacements from individual interferograms,
- $\alpha_1, \alpha_2, \dots, \alpha_n$ – incidence angle (from 20 to 46 degrees for SENTINEL),
- $\theta_1, \theta_2, \dots, \theta_n$ – orbit deviation angle from the direction of the coordinate system (for SENTINEL, –15 degrees for ascending orbit and –165 degrees for descending orbit),
- U_{WE}, U_{SN}, U_H – displacements in the directions of the coordinate system (for example, aligned with the geodetic coordinate system).

The paper employs the mathematical coordinate system in line with the practice for deformation research in mining areas. The west-east axis is labelled X , and displacements are labelled U . The south-north axis is labelled Y , and displacements in this direction are labelled V . The axis perpendicular to the surface is labelled Z , and vertical displacements are labelled S . As the investigated problem concerns subsidence, downward vertical displacements are traditionally positive, while upward displacements are negative.

Eq. (1) is a classic system of n equations with three unknowns solved with matrices. Regrettably, SENTINEL imagery offers only two satellites, 1A and 1B. Also, due to the heading angle values α adopted for Sentinel-1 (near-polar orbit), the N-S component is estimated with significant error, even when data from several different geometries are available. Thus, a common approach is to ignore the N-S component when deriving displacement components from multiple geometries. This gives only two equations. Considering the angle between the orbits and the coordinate system, the LOS signal can be decomposed to compute displacement along the X and Z axes. The procedure for determining components of the displacement field from mining-induced tremors is presented in the diagram in Fig. 2.

The diagram in Fig. 2 shows the path from LOS displacement maps to the description of tremor-induced surface displacement geometry. The first part of the diagram covers the determination of displacement vectors and can be applied to various deformation phenomena. The present

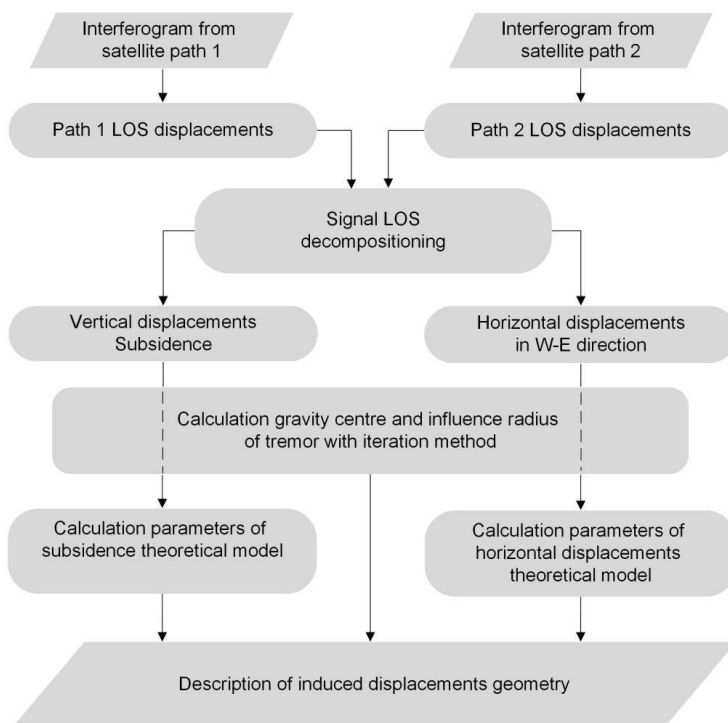


Fig. 2. Determination of tremor geometry from two InSAR images

paper focuses on mining-induced tremors. It is what the other part of the diagram covers. With remotely sensed displacements as the starting point, one can attempt to describe theoretically the displacement field caused by tremors. It entails the description of geometric parameters of the theoretical model of the displacement field formation.

Mining-induced tremors are caused by various mining and geological factors related to mineral exploitation [39,40]. Many hypotheses for tremor origins have been proposed [41,42]. Mining changes rock mass stress arrangements where substantial elastic strain energy is stored. After a certain threshold is exceeded, the energy is released. Therefore, the tremor potential is affected mainly by the parameters of the rock around the excavation (rock strength, ability to accumulate and release energy, etc.).

The present paper describes the tremor-induced deformation process using images from a copper ore mining site in the Legnica-Głogów Copper District (LGCD) [43]. KGHM PM S.A. has been mining the area since the 1960s. The activity affects many square kilometres of surface. The mining depths are significant, from 400 to 1200 m. It is a single-seam deposit mined using the room and pillar method [43]. Apart from direct deformations, the area has been affected by indirect ones. Water is withdrawn from the rock mass, causing a large-area drainage trough. Paraseismic tremors have become an inherent part of mining activities in LGMD, and the area experiences several dozen tremors of diverse energy parameters a year.

The paper focuses on two of them, Tremor_A (December 2017) and Tremor_B (November 2016). The time intervals between SAR images used to map displacements are several days.

Fig. 3 below shows the shaping of the displacement field caused by each tremor. An approximate range radius of 1000 m was used (for larger distances there is a significant impact of random scattering). The grey contour marks the outline of the mining activities area, while tremor epicentres (determined from multiple sources) are marked in red. The epicentres were acquired from the EPOS research project and the mine operator, KGHM.

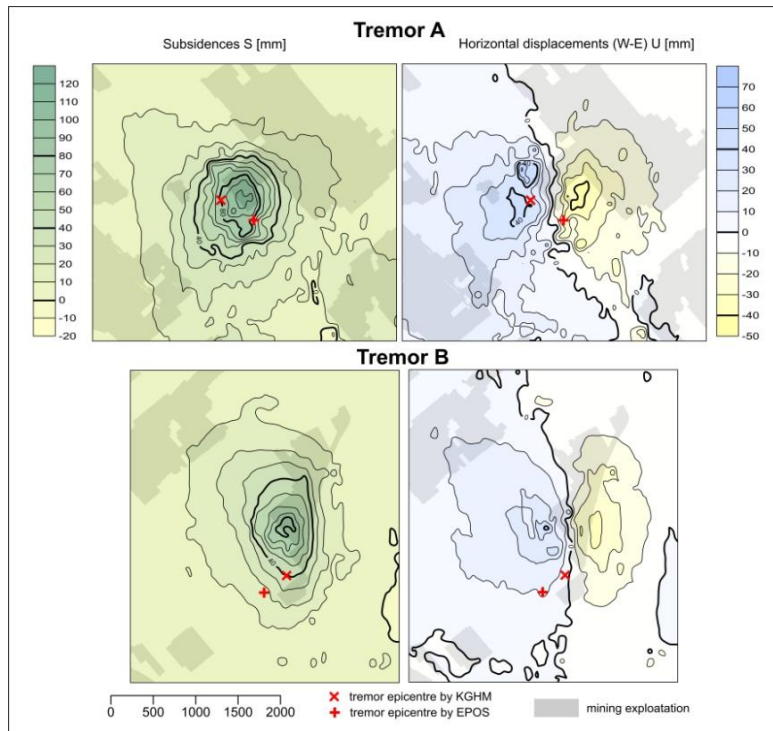


Fig. 3. Vertical S and horizontal U displacements caused by Tremors

Tremor_A caused a displacement field in the area of mining activity. Directions of horizontal displacements and arrangement of subsidies unambiguously demonstrate that the displacements form a subsidence trough. The maximum vertical displacements in the trough reach about 105 mm. The maximum horizontal displacements were about +60 mm (west to east) and -50 mm (east to west). Both epicentres are situated in the subsidence trough but several hundred metres from its bottom. The convergence point for points on the surface is referred to as the centre of gravity. In the case of indirect deformations, displacement vectors are directed towards the centre of gravity of the subsidence trough as well [44-46].

Tremor_B also caused a displacement field in the form of a subsidence trough. The maximum vertical displacements were about 85 mm, while horizontal displacements reached -35 mm (east to west) and +40 mm (west to east). The shape of this trough is elongated along the north-south direction. The epicentres of this tremor are significantly shifted to the south compared to the centre of the subsidence trough.

The shapes of the resulting displacement field show that mining-induced tremors caused relatively regular subsidence troughs. Furthermore, horizontal displacements indicate that surface points are shifted towards the bottoms of the troughs. A comparable geometric effect was observed in the research on stochastic medium models [47]. Therefore, further analysis is founded on the theoretical model of slot release in a stochastic medium.

3. Slot release

Model research on the displacement field generated by a mining-induced void gained popularity in the mid-twentieth century. It was related to the possibility of repeating model tests for the same assumed conditions, which was impossible in mining practice. Model research was pursued in various academic centres. Three different laboratory models of a deforming medium were applied:

- ‘sand’ model (stochastic) [48,49],
- ‘gel’ model (elastic) [50,51],
- analogue model [52,53].

Led by Litwiniszyn and Knothe, the Strata Mechanics Research Institute of the Polish Academy of Sciences conducted intensive model research [47,49,54-56]. The results were used to research the theory for deformation forecasting [57]. A model box – with front and back walls made of glass – was filled with fine sand, and measuring points were placed on top. Next, a slot in the bottom of the box was opened to release the sand. Finally, the moving medium was photographed [49,54]. The results allowed the researchers to form equations to describe vertical and horizontal sand displacement. The studies were conducted for flat deformations (2D). Their results were consistent with the theoretical hypotheses of the stochastic theory [58].

Extrapolating results for a flat model (slot release) onto a spatial model (point release), the displacement equations can be:

- for vertical displacements:

$$S = S_m \exp \left[-\pi \frac{(x-x_0)^2 + (y-y_0)^2}{r_S^2} \right] \quad (2)$$

- for horizontal displacements:

$$\begin{aligned} U &= -U_m \frac{x-x_0}{r_U} \exp \left[-\pi \frac{(x-x_0)^2 + (y-y_0)^2}{r_U^2} \right] \\ V &= -U_m \frac{y-y_0}{r_U} \exp \left[-\pi \frac{(x-x_0)^2 + (y-y_0)^2}{r_U^2} \right] \end{aligned} \quad (3)$$

where:

- S_m, U_m – parameters of the theoretical model for maximum displacements,
- r_S, r_U – parameters of the theoretical model for vertical and horizontal displacement ranges, respectively
- x_0, y_0 – 2D coordinates of the centre of gravity towards which surface points are shifted (point of release).

Assuming that the formation process of a displacement field caused by mining-induced tremors is analogous to the formation of a direct displacement field (the same distortion propagation medium), one can use observations for direct displacements. Therefore, let us assume that

- the range radii of the displacements are the same $r = r_S = r_U$,
- Aviershin's [59] observation concerning direct proportionality between horizontal displacements and the derivative of vertical displacements is true:

$$U = -B \frac{\partial S}{\partial x} \quad (4)$$

$$V = -B \frac{\partial S}{\partial y}$$

- the coordinate system origin is located in the centre of gravity.

Hence, Eqs. (2) and (3) take the following forms:

$$S = S_m \exp \left[-\pi \frac{d^2}{r^2} \right] \quad (5)$$

$$U = -U_m \frac{x}{r} \exp \left[-\pi \frac{d^2}{r^2} \right] \quad (6)$$

$$V = -U_m \frac{y}{r} \exp \left[-\pi \frac{d^2}{r^2} \right]$$

where d is the distance of the computational point to the centre of gravity.

If Eq. (6) and differential coefficient of (5) with respect to x is substituted into Eq. (4).

$$B = -\frac{U_m r}{S_m 2\pi} \quad (7)$$

Note that Aviershin [59] referred the value of parameter B to the mining depth and proposed $0.16H$, while for Polish mining conditions, Budryk [60] proposed to relate the parameter to the range radius of impacts of Knothe's theory [61] with the value of $0.40r$. The variability of the coefficient for LGMD was investigated by Kwinta et al. [62] and Hejmanowski and Kwinta [63].

Eqs. (5) and (6) can be plotted as shown in Fig. 4. The 'release point' or the centre of gravity is marked in red.

Figs. 3 and 4 exhibit certain significant similarities. Actual displacements are not 'perfectly' fitted to theoretical displacements. The differences probably stem from the probabilistic and deterministic course of the deformation process, but the theoretical model considers only the deterministic part of the process. Therefore, one can assume for further computations that the point release model correctly describes the distribution of surface displacements from a mining-induced tremor.

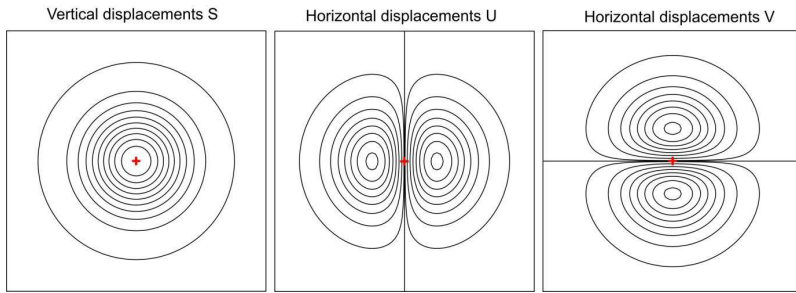


Fig. 4. Vertical and horizontal displacement isolines for point release

4. Case studies

The study now proceeds to compute geometric parameters of the displacement field as per the procedure in Fig. 2. First, the centre of gravity for the displacements had to be determined. An analysis of Figs. 4 and 5 suggested serious potential errors if coordinates of the epicentres

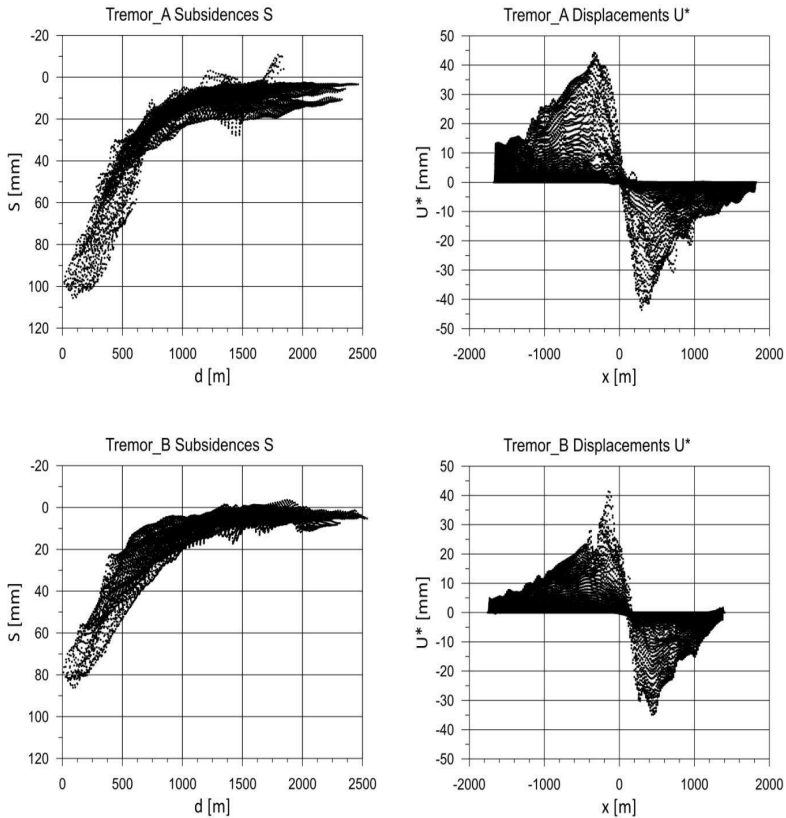


Fig. 5. Distribution of displacements as a function of distance to the centre of gravity

were used. Therefore, the centre of gravity was identified with squares of vertical displacements (weighted mean). Fig. 5 presents vertical displacements as a function of distance to the centre of gravity and adjusted horizontal displacements as a function of coordinate x (3D to 2D transition).

Horizontal displacements were adjusted by the factor related to the distance to the x -axis to represent them in the plot (8). An approximate range radius of 1000 m was utilised, which results from the shape of the measured subsidence troughs (Fig. 3). This value does not significantly affect the result of the calculation, and increasing it only increases the dispersion of the final result.

$$U^* = U \exp \left[-\pi \frac{y^2}{r^2} \right] \quad (8)$$

Vertical displacement plots show that the resulting bandwidth depends on the degree of deformation distortion. A large number of points far from the subsidence trough centre disturbs the geometric description of the displacements. There is also a systemic factor. Therefore, the theoretical Eq. (5) has to be modified to (9):

$$S = S_m \exp \left[-\pi \frac{d^2}{r^2} \right] + S_0 \quad (9)$$

In the case of adjusted horizontal displacements, there are many points with minor displacement values (outside the range of significant displacement). The zero is shifted outside the centre of gravity. There is a systemic factor as well. The modified theoretical Eq. (6) becomes (10):

$$U^* = -U_m \frac{x}{r} \exp \left[-\pi \frac{x^2}{r^2} \right] + U_0 \text{sign}(x) \quad (10)$$

As the impact range radius affects the centre of gravity, and the centre of gravity affects the impact range radius, computations were iterative. As per the diagram in Fig. 2, the y coordinate of the centre of gravity was calculated iteratively based on vertical displacements, and horizontal displacements were used to determine the x coordinate. The stopping criterion for the iterative process was if changes in the centre of gravity's coordinates fell below 1 metre.

The case study was performed in 2D for simplicity's sake. Additionally, this approach takes into account the substantial impact of points in the central part of the displacement field when determining its geometric parameters. The distance to the centre of gravity was divided into 50-metre intervals where mean displacements were computed. The method for horizontal displacements was weighted mean, where the weight was the squared distance to the x -axis. Finally, the centre of gravity and the mean impact range radius were calculated for each case. Fig. 6 shows results for Tremor A and Tremor B. The analysis covered displacements up to $1.5r$ from the centre of gravity due to the theoretical function behaviour (further displacements are negligible).

Geometric parameters of the model of a theoretical displacement field were determined by the provided methods. First, parameters for vertical displacements were determined independently with Eq. (9). Then, the same was conducted for horizontal displacements, Eq. (10). Then, the impact range radius was set to equal the mean from vertical and horizontal displacements in line with previous assumptions. Consequently, the theoretical models required two parameters each for vertical and horizontal displacements that needed to be determined. The parameters of the

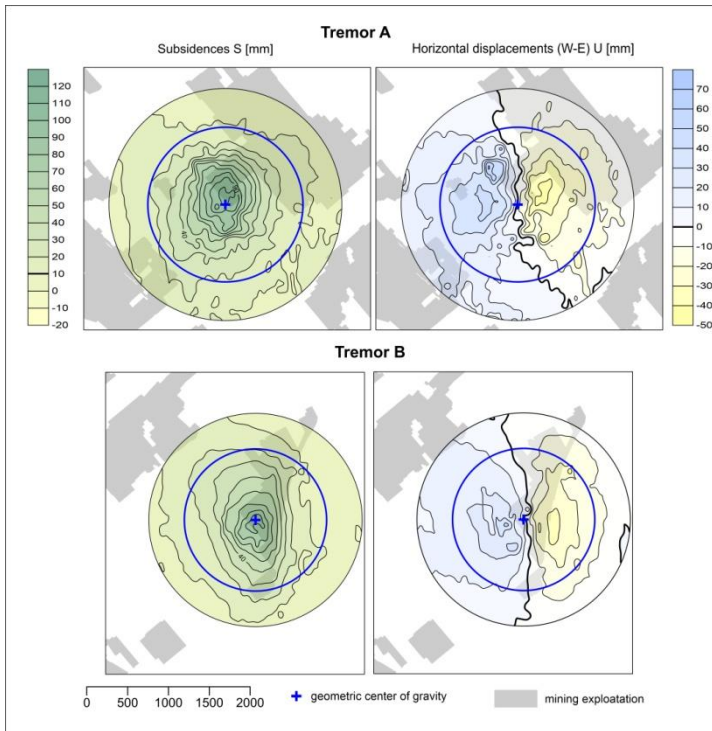


Fig. 6. Determination of the centre of gravity and impact range radius for Tremor A and B

theoretical models of displacements were computed in Grapher by Golden Software. The fit of the theoretical curves to the measured points is shown in Fig. 7. Black points are mean displacements from the computation ranges. The red line is the deformation according to the parameters of the computational models.

The parameters of the theoretical models are summarised in TABLE 1. It also presents values of the measure of fit, R -squares for vertical displacements (R_S^2) and horizontal displacements (R_U^2).

TABLE 1

Summary of computed geometric parameters of the theoretical models

Parameter	Tremor A	Tremor B
r [m]	949	871
S_m [mm]	87.5	68.8
S_0 [mm]	10.0	9.6
R_S^2	0.9980	0.9904
U_m [mm]	104.9	88.4
U_0 [mm]	-12.7	-7.9
R_U^2	0.9506	0.9624
B [m]	0.17H (0.19r)	0.15H (0.20r)

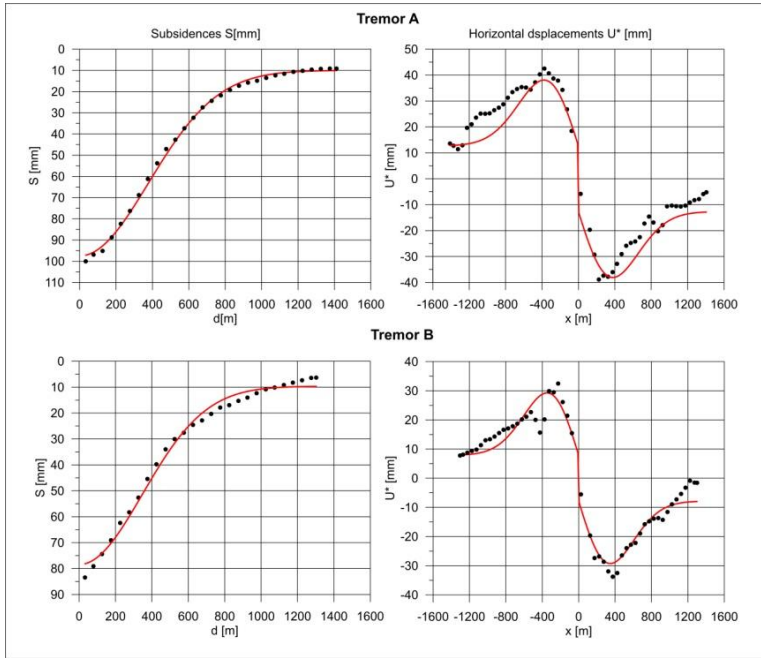


Fig. 7. Fitting the theoretical models to the displacements for Tremor A and B

The results in TABLE 1 and Fig. 7 show very high goodness of fit of the theoretical displacements to the ‘measured’ ones. The fit of vertical displacements is better than for horizontal ones. The range radii are large. Direct impact range radii in this mining area are minor. A constant displacement factor is present for vertical and horizontal displacements. The calculations show that values of vertical displacements are about 10 mm too high for both tremors. Likewise, a systemic factor was detected for horizontal displacements, but it varied between the tremors. The systemic factor for Tremor_A was about 13 mm, and for Tremor_B, about 8 mm. TABLE 1 also includes results of Aviershin’s B coefficient (1947). They are consistent with values proposed by Aviershin but smaller than average values used for direct deformations in LGMD [63].

A comparison of the results of measured and theoretical displacements (tremors A and B) can be shown in Fig. 8. Vertical displacements S were determined according to relation (9), while horizontal displacements were determined according to relation (11):

$$U = -U_m \frac{x}{r} \exp \left[-\pi \frac{d^2}{r^2} \right] + U_0 \operatorname{sign}(x) \quad (11)$$

The calculations included the parameter values summarised in TABLE 1. For each case and each displacement, the difference between the measured (InSAR) and calculated (model) displacements is shown.

Differences between measured values (InSAR) and model values may be due to the erroneous assumption of non-occurrence of displacements in the NS direction for measured data (distortion of the true displacement picture).

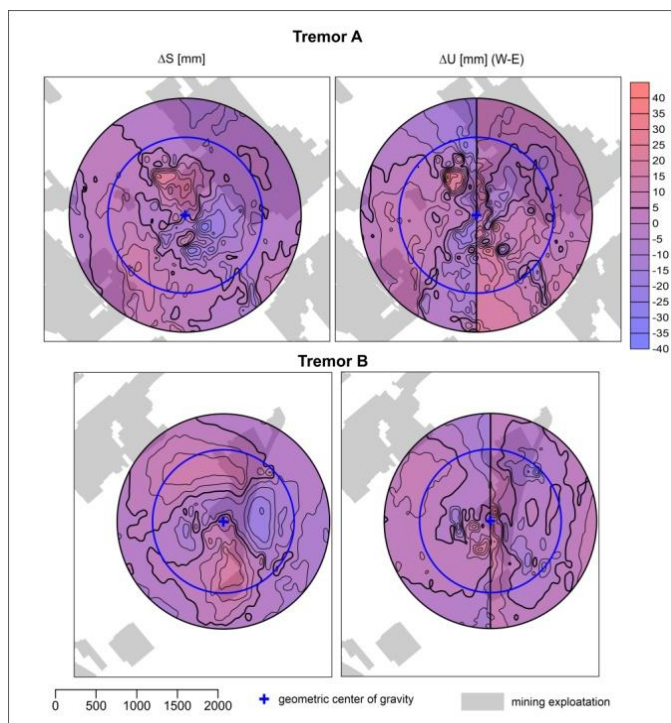


Fig. 8. Differences between measured and theoretical displacements – tremors A and B

5. Summary

Underground mining causes surface deformation. It can progress gradually over extended periods or happen rather dynamically. Surface displacements caused by mining-induced tremors are among those dynamic phenomena. A permanent displacement field (subsidence trough) in the tremor area can damage objects on the surface. Such a subsidence trough caused by a tremor is linked to a mining void in the rock mass. Science has yet to learn how to predict parameters of such tremor-induced subsidence troughs. Nevertheless, a past dynamic event (tremor) can be used to determine geometric parameters of its effects (a displacement field).

The present paper described a tremor-induced displacement field with a displacement model used in stochastic medium modelling, Eqs. (4)-(6). The model can determine the reach of the subsidence trough based on the impact range radius r and identify the dependence between horizontal and vertical displacements with Aviershin's model. The results of the fit of the theoretical model to the displacement field from InSAR data demonstrated the correctness of the theoretical model. The R-squared fit measures are excellent.

The computations determined the most probable centres of gravity of the subsidence troughs (Fig 6) towards which points on the surface move. The B coefficient determines the vertical coordinate of the subsidence trough's centre of gravity.

The study identified systemic factors for displacement distributions that result in displacement values about 10% higher despite the reduction of tropospheric effects and should be removed

when LOS displacements are determined. Furthermore, the determined differences between the measured values and the model show the influence of omitting the horizontal component of the NS during the decomposition of the LOS signal.

The results are very interesting, and more cases should be analysed and juxtaposed with results for direct displacements. Another interesting future research would be to look for relations between tremor epicentres recorded with geophysical instruments and the location of the centre of gravity of a subsidence trough according to remote sensing data. Such research can undoubtedly contribute to a better understanding of the physics behind deformations caused by mining-induced tremors.

References

- [1] H. Kratzsch, Mining Subsidence Engineering. Springer-Verlag Berlin Heidelberg New York (1983).
- [2] J. Blachowski, W. Milczarek, P. Stefaniak, Deformation information system for facilitating studies of mining ground deformations - development and applications. *Natural Hazards and Earth System Sciences* **14**, 1677-1689 (2014).
- [3] D. Galloway, T. Burbey, Review: regional land subsidence accompanying groundwater extraction. *Hydrogeology Journal* **19** (8), (2011).
- [4] P. Pasquali, A. Cantone, P. Riccardi, M. De Filippi, F. Ogushi, M. Tamura, S. Gagliano, Monitoring land subsidence in the Tokyo region with SAR interferometric stacking techniques. In *Engineering Geology for Society and Territory*; Springer: Berlin/Heidelberg, Germany **5**, 995-999 (2015).
- [5] P. Castellazzi, N. Arroyo-Domínguez, R. Martel, A.I. Calderhead, J.C. Normand, J. Gárfias, A. Rivera, Land subsidence in major cities of Central Mexico: Interpreting InSAR-derived land subsidence mapping with hydrogeological data. *Int. J. Appl. Earth Obs. Geoinf.* **47**, 102-111 (2016).
- [6] YQ. Wang, ZF. Wang, WC. Cheng, A review on land subsidence caused by groundwater withdrawal in Xi'an, China. *Bull Eng Geol Environ* **78**, 2851-2863, (2019).
- [7] F. Cigna, D. Tapete, Urban Growth and Land Subsidence: Multi-Decadal Investigation Using Human Settlement Data and Satellite InSAR in Morelia, Mexico. *Sci. Total Environ.* **811**, 152211 (2022).
- [8] S. Karimzadeh, M. Ghasemi, M. Matsuoka, K. Yagi, A.C. Zulfikar, A deep learning model for road damage detection after an earthquake based on synthetic aperture radar (SAR) and field datasets. *IEEE J. Sel. Topics Appl. Earth Observ. Remote Sens.* **15**, 5753-5765 (2022).
- [9] S.S. Peng, Coal mine ground control. John Wiley & Sons. (1986).
- [10] Y.P. Chugh, Q.W. Hao, F.S. Zh, State of the art. In mine subsidence prediction. „Land Subsidence 1989” Publ. Balkema.
- [11] A. Malinowska, W. Witkowski, A. Guzy, R. Hejmanowski, Mapping ground movements caused by mining-induced earthquakes applying satellite radar interferometry. *Engineering Geology* **246**, 402-411 (2018).
- [12] W. Milczarek, Investigation of post induced seismic deformation of the 2016 MW 4.2 Tarnovek Poland mining tremor based on DInSAR and SBAS method. *Acta Geodyn. Geomater* **2**, 183-193 (2019).
- [13] W. Milczarek, A. Kopeć, D. Głabicki, N. Bugajska, Induced seismic events – distribution of ground surface displacements based on InSAR methods and Mogi and Yang models. *Remote Sensing* **13** (8), 1451 (2021).
- [14] K. Owczarż, J. Blachowski, Application of DInSAR and spatial statistics methods in analysis of surface displacements caused by induced tremors. *Applied Sciences (Switzerland)* **10** (21), 7660, 1-23 (2020).
- [15] B. Antonielli, A. Sciortino, S. Scancelli, F. Bozzano, P. Mazzanti, Tracking Deformation Processes at the Legnica Glogow Copper District (Poland) by Satellite InSAR – I: Room and Pillar Mine District. *Land* **10**, 653 (2021).
- [16] A. Kopeć, A. Kwinta, Osiadanie powierzchni terenu z tytułu szczyrpywania wody- wyznaczenie technikami InSAR. *Przegląd Górniczy* **1**, 27-32 (2019) (in Polish).
- [17] R. Hejmanowski, A. Malinowska, Evaluation of reliability of subsidence prediction based on spatial statistical analysis. *International Journal of Rock Mechanics and Mining Sciences* **46** (2), (2009).

- [18] A. Kwinta, R. Gradka, Mining exploitation influence range. *Natural Hazards* **94**, 3, 979-997 (2018).
- [19] A. Kwinta, R. Gradka, Analysis of the damage influence range generated by underground mining. *International Journal of Rock Mechanics and Mining Sciences* **128** (2020).
- [20] J.W. Borchers, M. Carpenter, Land Subsidence from Groundwater Use in California. California Water Foundation Full Report of Findings/April 2014
- [21] R. Hejmanowski, A. Kwinta, Implementation of GPS satelitary technique for monitoring of point displacements on mining areas. *Proceedings of Second World Mining Environment Congress*. **1**, 351-369, 13-16 May 1997, Katowice.
- [22] R. Hejmanowski, A. Kwinta, Measurement of horizontal displacements in European coalfields. In: 10th international symposium on Deformation measurements: Orange, California, USA (2001).
- [23] H. Zhao, F. Ma, Y. Zhang, Monitoring and Analysis of the Mining-Induced Ground Movement in the Longshou Mine, China. *Rock Mechanics and Rock Engineering* **46**, 207-211 (2013).
- [24] Z. Szczerbowski, J. Jura, Mining induced seismic events and surface deformations monitored by GPS permanent stations. *Acta Geodyn. Geomater.* **12**, 3 (179), 237-248 (2015).
- [25] T. Gargula, A. Kwinta, Z. Siejka, Zastosowanie sieci modularnych zintegrowanych z pomiarami GPS do wyznaczenia przemieszczeń. *Materiały konferencji „III Ogólnopolska konferencja naukowo techniczna: Kartografia numeryczna i informatyka geodezyjna”*, Rzeszów, 93-104, (2009) (in Polish).
- [26] Z. Perski, Applicability of ERS-1 and ERS-2 InSAR for land subsidence monitoring in the Silesian coal mining region, Poland. *International Archives of Photogrammetry and Remote Sensing* **32**, 555-558 (1998).
- [27] L. Ge, H.C. Chang, C. Rizos, Mine subsidence monitoring using multi-source satellite SAR images. *Photogrammetric Engineering & Remote Sensing* **73** (3), 259-266 (2007).
- [28] J. Blachowski, E. Jiráňková, M. Lazecký, P. Kadlečík, W. Milczarek, Application of Satellite Radar Interferometry (PSInSAR) in Analysis of Secondary Surface Deformations in Mining Areas. *Case Studies from Czech Republic and Poland. Acta Geodyn. Geomater.* **5**, 2, 173-185 (2018).
- [29] C. Carnec, D. Massonnet, C. King, Two examples of the use of SAR interferometry on displacement fields of small spatial extent. *Geophysical Research Letters* **23**, 3579-3582 (1996). DOI: <https://doi.org/10.1029/96gl03042>
- [30] W.T. Witkowski, D. Mrocheń, P. Sopata, T. Stoch, Integration of the Leveling Observations and PSInSAR Results for Monitoring Deformations Caused by Underground Mining, 2021 IEEE International Geoscience and Remote Sensing Symposium IGARSS, 6614-6617, (2021).
- [31] P. Sopata, T. Stoch, A. Wójcik, D. Mrocheń, Land Surface Subsidence Due to Mining-Induced Tremors in the Upper Silesian Coal Basin (Poland) – Case Study. *Remote Sensing* **12** (23), 3923 (2020).
- [32] C. Jiang, L. Wang, X. Yu, S. Chi, T. Wei, X. Wang, DPIM-Based InSAR Phase Unwrapping Model and a 3D Mining-Induced Surface Deformation Extracting Method: A Case of Huainan Mining Area. *KSCE J. Civ. Eng.* **25**, 654-668 (2021). DOI: <https://doi.org/10.1007/s12205-020-5288-0>
- [33] A. Kopeć, N. Bugajska, W. Milczarek, D. Głębicki, Long-term monitoring of the impact of the impact of mining operations on the ground surface at the regional scale based on the InSAR-SBAS technique, the Upper Silesian Coal Basin (Poland). *Case study. Acta Geodynamica et Geomateriali* 93-110 (2022). DOI: <https://doi.org/10.13168/AGG.2021.0044>
- [34] A. Kopeć, Metodyka przetwarzania danych interferometrycznych w aspekcie oddziaływania podziemnej eksploatacji górniczej na powierzchnię terenu. *Politechnika Wroclawska. Wrocław*, (2021). (PhD thesis).
- [35] D. Sandwell, R. Mellors, X. Tong, M. Wei, P. Wessel, GMTSAR: An InSAR Processing System Based on Generic Mapping Tools. (2011).
- [36] C.W. Chen, H.A. Zebker, Network approaches to two-dimensional phase unwrapping: intractability and two new algorithms. *J. Opt. Soc. Am. A, JOSAA* **17**, 401-414 (2000). DOI: <https://doi.org/10.1364/josaa.17.000401>
- [37] C.W. Chen, H.A. Zebker, Two-dimensional phase unwrapping with use of statistical models for cost functions in nonlinear optimization. *J. Opt. Soc. Am. A, JOSAA* **18**, 338-351 (2001). DOI: <https://doi.org/10.1364/josaa.18.000338>
- [38] C. Yu, Z. Li, N.T. Penna, P. Crippa, Generic Atmospheric Correction Model for Interferometric Synthetic Aperture Radar Observations. *Journal of Geophysical Research: Solid Earth* **123**, 9202-9222 (2018). DOI: <https://doi.org/10.1029/2017jb015305>

- [39] P.L. Swanson, C.D. Sines, Characteristics of mining-induced seismicity and rock bursting in a deep hard-rock mine. Report of Investigations, US. Dept. of the Interior, Bureau of Mines, (1991). No. 9393.
- [40] J. Butra, J. Kudelko, Rockburst hazard evaluation and prevention methods in Polish copper mines. *Cuprum* **61**, 5-20 (2011).
- [41] I.W. Wong, Recent developments in rockburst and mine seismicity research. Proceedings of 33rd U.S. Symposium on Rock Mechanics. (ed. by Tillerson & Wawersik). A.A. Balkema, Rotterdam, 1103-1112 (1992).
- [42] X.T. Feng, Rock Mechanics and Engineering: Volume I: Principles (1st ed.). CRC Press. (2017).
- [43] W. Salski, The tectonics of the deposit. In: Monografia KGHM Polska, Miedź, S.A. and Piestrzyński, A. (eds.). Pub. Profil, Kraków, (1996). (in Polish).
- [44] O. Niemczyk, Zur Frage des Grenz- und Bruchwinkels bei Bodensenkungen. Mitt. Aus dem Markscheidewesen, Stuttgart, (1935) (in Germany).
- [45] A. Kwinta, Weryfikacja modeli niestacjonarnego pola poziomych przemieszczeń górniczych. Akademia Górniczo-Hutnicza. Kraków, (2003) (PhD thesis).
- [46] K. Tajduś, Analysis of horizontal displacement distribution caused by single advancing longwall panel excavation. *Journal of Rock Mechanics and Geotechnical Engineering* **7**, 395-403 (2015).
- [47] D. Krzyszoń, Parametr zasięgu niecek Osiedlenia. *Archiwum Górnictwa* **10**, 1, Warszawa, (1965), (in Polish)
- [48] D. Krzyszoń, Dispersion Parameter of Elementary Subsidence Throughs inside a Loose Medium. *Biul. PAN, S. Nauk Technicznych* **11**, Nr 10, Kraków (1963).
- [49] D. Krzyszoń, L. Rogowski, Experimental Investigation of a Stochastic Discontinuously Non-homogeneous Medium. *Biul. PAN, S. Nauk Technicznych* **8**, Nr 6, Kraków (1960).
- [50] A. Dunikowski, Punktowa metoda wyznaczania przemieszczeń w ośrodku sprężystym pozostającym pod działaniem sił masowych. *Archiwum Górnictwa* **1**, z.1, Warszawa, (1956), (in Polish)
- [51] H.J. King, J.T. Whetton, Mechanics of mine subsidence. Proceedings of the European Congress on Ground Movement, Leeds 27/36 (1957).
- [52] B. Drzęźła, Badania teoretyczne i modelowe ruchów górotworu przy eksploatacji górniczej. Politechnika Śląska, Gliwice, (1971). (PhD thesis).
- [53] H. Koyi, Analogue modelling; from a qualitative to a quantitative technique, a historical outline. *Journal of Petroleum Geology* **20**, 233-238 (1997).
- [54] J. Rogowska, Badania eksperymentalne niecek osiedlenia w ośrodku sypkim z uwzględnieniem zmiany gęstości ośrodka. Polska Akademia Nauk, Kraków (1973) (PhD thesis).
- [55] J. Litwiniszyn, O niektórych liniowych i nieliniowych modelach niecki osiedlenia w górotworze sypkim. *Przegląd Górniczy* **18**, 5, Katowice (1962) (in Polish).
- [56] J. Litwiniszyn, A remark concerning the so called „point of the attraction centre” and its connection with the formation of the subsidence trough. *Archiwum Górnictwa* **19**, 3, Warszawa (1974).
- [57] S. Knothe, J. Leśniak, W. Pielok, W. Rogowska, The subsidence of rock mass caused by mining exploitation. The model testing. Proceedings of the International Mining Tech'95 Symposium 4-6 October 1995, Beijing (in Polish).
- [58] J. Litwiniszyn, Równanie różniczkowe przemieszczeń górotworu. *Archiwum Górnictwa i Hutnictwa* **1**, 1, Warszawa (1953) (in Polish).
- [59] S.G. Avershin, Sdwiżeniye gornych porod pri podziemnykh razrabotkach. Ugleteichzdat, Moskwa, (1947) (in Russian).
- [60] W. Budryk, Wyznaczanie wielkości poziomych odkształceń terenu. *Archiwum Górnictwa i Hutnictwa* **1**, 1, Warszawa (1953) (in Polish).
- [61] S. Knothe, Równanie profilu ostatecznie wykształconej niecki osiedlenia. *Archiwum Górnictwa i Hutnictwa* **1**, 1, Warszawa (1953) (in Polish).
- [62] A. Kwinta, R. Hejmanowski, G. Patykowski, Metoda wyznaczania współczynnika proporcjonalności przemieszczeń poziomych B dla rejonu O/ZG „Lubin”. Materiały konferencji „VIII Dni Miernictwa Górniczego i Ochrony Terenów Górniczych”, Ustroń, 324-333, (2005), (in Polish).
- [63] R. Hejmanowski, A. Kwinta, Determining the Coefficient of Horizontal Displacements with the Use of Orthogonal Polynomials. *Archives of Mining Sciences* **54**, 3, 441-454 (2009).